Spark Plasma Extrusion and the Thermal Barrier Concept

L. ČELKO, M. MENELAOU, M. CASAS-LUNA, M. HORYNOVÁ, T. MUSÁLEK, M. REMEŠOVÁ, S. DÍAZ-DE-LA-TORRE, K. MORSI, and J. KAISER

Spark plasma sintering (SPS) is currently a major powder consolidation process with many advantages; however, it is still largely limited to the processing of simple shapes such as discs due to its geometric restrictions. Alternatively, spark plasma extrusion (SPE) is a recently developed process that has superiority over SPS in terms of faster consolidation, generating products of extended geometries and potential grain refinement capabilities under applied current. So far, work on SPE has resulted in large temperature gradients within the extruding material with microstructural and properties in-homogeneities. The present paper reports on a novel approach (thermal barrier concept) that allows the SPE of materials with enhanced uniformity in terms of microstructures and properties. Both aluminum and aluminum-carbon nanotube composites have been successfully processed using this new approach.

https://doi.org/10.1007/s11663-018-1493-3

I. INTRODUCTION

SPARK plasma sintering (SPS), also often referred as Pulsed Electric Current Sintering (PECS), Field-Assisted Sintering Technique (FAST), or Electric Current-Activated Sintering (ECAS), has been a known technology for almost four decades and is still studied worldwide. A detailed description of this technology is given in a review paper by Orrú *et al.*[1] This interesting technology is highly motivated by rapid solid-state sintering for a various number of initial powder materials such as ceramics, intermetallics, metals, and/or their composites. For example, hetero-nanostructured FeAl metallic materials were successfully produced *via* SPS by Grosdidier *et al.*[2] and in a detailed review Munir *et al.*[3] studied SPS of intermetallic and ceramic materials under the influence of high heating rate, pressure, and current. Tokita[4] discussed the SPS of tungsten carbides which have uses as molds, press stamping dies, cutting tools, and machine components. Hussein *et al.*[5] obtained nano-grained Ti-Nb-Zr alloys through SPS with dental and orthopedic applications. In addition, Kim *et al.*[6] studied the conduction character of Y_2O_3-SiC specimens for the development of ceramic electric conductors and Mudinepalli *et al.* investigated perovskite ferroelectric-based materials with enhanced magnetoelectric properties potentially used in piezoelectric devices.[7] Modifications in SPS process parameters enable the manufacture of materials with different properties. Tokita was one of the first to study the influence of temperature and pressure in order to obtain functionally graded materials (YSZ/steel).[8] In addition, Wang *et al.* theoretically and experimentally studied how temperature and stress can affect the densification with respect to electrical potential.[9] Despite the relatively large effort already being expended in the field of SPS process as Grasso *et al.* summarized, most of the studies are still mainly focused on the production of simple disc-shaped samples using conventional design of graphite containers.[10]

Only a limited number of publications were found that are related to enhanced properties in sintered materials, using re-design shape of the graphite container and/or the SPS process itself. For example, Tokita developed an automated electrical sintering process with the aim of processing directly functionally graded materials based on the container wall thickness variations (*i.e.,* temperature distribution changes, enabled production of samples with different level of porosities).[11] Lichtinghagen patented a continuous extrusion device using electric current to heat and extrude electrically conductive granulated materials.[12]

L. ČELKO, M. MENELAOU, M. CASAS-LUNA, M. HORYNOVÁ, M. REMEŠOVÁ, and J. KAISER are with the CEITEC Central European Institute of Technology, Brno University of Technology, Purkynova 123, 612 00 Brno, Czech Republic. Contact e-mail: ladislav.celko@ceitec.vutbr.cz T. MUSÁLEK is with the Activair s.r.o. Sadová 44, 746 01 Opava, Czech Republic. S. DÍAZ-DE-LA-TORRE is with the CIITEC Instituto Politécnico Nacional, Centro de Investigación e Innovación Tecnológica, Cerrada de Cecati, Colonia Santa Catarina, Azcapotzalco, 02250 Mexico D.F., Mexico. K. MORSI is with the Department of Mechanical Engineering, San Diego State University, 5500 Campanile Drive, San Diego, CA 92182.

Manuscript submitted October 21, 2018.

Published online: 02 January 2019

Morsi *et al.*[13] published the first research paper on what is known today as spark plasma extrusion (SPE), which involves the simultaneous extrusion and consolidation of powders under the influence of electric current in a single step. Very recently, Novitskaya *et al.*,[14] used this process to study the devitrification behavior of Fe-based amorphous metal containing Y_2O_3 nanoparticles.

The SPE process offers a promising alternative to scaling and potentially to the industrial use of the current-assisted sintering process, in order to produce materials with extended geometries and enhanced characteristics. Morsi *et al.*[13] claimed that recrystallization of sintered powder materials under the influence of electric current, can lead to grain size refinement *via* the SPE process; at present, this is not possible using the conventional SPS technique. Also, Morsi *et al.*[15] reported the successful consolidation and extrusion by means of SPE of both aluminum and aluminum-carbon nanotubes. The work on SPE has so far been conducted in a specialized spark extrusion rig (not available commercially), with the extrusion container initially maintained at room temperature. This can promote the rapid cooling of the extruding material during the actual extrusion process, resulting in substantial variation in grain size of the extruded material along its length. The ability to use existing SPS equipment to execute SPE studies has not yet been extensively reported, which could open the door for SPS researchers to further investigate unlimited aspects of this new intriguing SPE process.

Hence, herein we are focused on theoretical and experimental research approaches in order to describe in detail the modification of SPS to allow SPE studies as well as to introduce the thermal barrier concept within the context of SPE. Thus, based on our observations, the thermal barrier concept is proven to be easily transferable to any other type of material (including metallic and/or metal matrix composites) regardless of the melting point of each material, and it can also enable a reproducible way to use the SPE technique towards any other commercially available SPS device. Results show the successful processing of aluminum-carbon nanotube composites using the new SPE approach.

II. EXPERIMENTAL PROCEDURE

Three grams of pure aluminum powder containing 3 vol pct of multiwall-carbon nanotubes, Al-CNTs which was purchased from ACN (Applied Carbon Nano Technology Co., Korea), were cold compacted in a standard SPS graphite container as it is shown in Figure 1(a). Uniaxial pressure of 32 MPa was used to produce the Al-CNTs green powder compacts for the SPE process under 15 Pa vacuum atmosphere. The cold press Al-CNTs samples were of 10 mm in diameter and 15 mm in height. The modified graphite container for SPE was designed and manufactured to allow a reduction in diameter from 10 to 5 mm upon exiting the container. (*i.e.,* extrusion ratio 4:1, using a conical container arrangement of angle 45 deg, which helps reduce extrusion pressure requirements). Note, that the container land was designed to be longer than that for the previous SPE rig, in order to provide strength for the graphite container arrangement and guarantee the straightness of the extruded part, also graphite can act as a lubricant in extrusion.

After the Al-CNTs green compacts were produced in the SPS container, they were each placed into the SPE container as shown in Figure 1(b). Two sets of samples were prepared; graphite paper was inserted between the punch and cold pressed Al-CNTs green compact for the first, while for the second, graphite paper was inserted between the punch and a layer of yttria partially stabilized zirconia (YSZ) powder (40.23.1, GTV GmbH, Germany), as well as between the layer of YSZ powder and cold pressed Al-CNTs green compact. The SPE container was surrounded by a thermal insulation felt and placed inside the working chamber of the commercially available SPS machine (DR.SINTER® model SPS1050, co. Sumitomo Coal & Mining Ltd.).

Once the high vacuum (~ 10 Pa) in the chamber was achieved and a DC pulse sequence of 12:2 was applied in order to allow Joule heating of the graphite container/setup. The current was gradually increased by a controller to allow heating to the extrusion temperature of 580 °C in 480 seconds. Within this heating cycle, the samples were subjected to a dwell of 120 seconds at a temperature of 200 °C to ensure the evaporation of all organic compounds (due to the powder cleaning and degreasing period), followed by heating to the extrusion temperature (580 °C). The graphite container temperature was measured using a K-type thermocouple, firmly located at the central part of the graphite container, *i.e.,* in the vicinity of the area reduction zone for extrusion. Simultaneously, temperature on the center of the upper punch was measured by means of pyrometer (Ircon ULTIMAX Plus UX-SW40). As soon as the extrusion temperature was reached in the graphite container, namely, 580 °C, then the pressure on the top punch was gradually increased in order to enable the extrusion process of Al-CNTs through the reduction zone. As a result, powder consolidation conditions were achieved simultaneously under the influence of the electrical pulse current. Extrusion was terminated when the z-axis displacement of 15 mm was reached (average speed = 0.01 mm/s).

Preliminary finite element analyses were conducted to gain an insight into the temperature distributions during SPE and confirm the experimentally determined temperature measurements. The finite element method (FEM) numerical calculations were performed in extremely fine physics controlled mesh of COMSOL Multiphysics software. The steady-state 2D axisymmetric geometry study with coupled electromagnetic and heat transfer modules was achieved in order to implement Joule heating effect (excluding, however, the heat rise due to work of extrusion which is the subject of a more detailed follow-up study). Also, it is driven by laws of conservation for electric charge and energy. The solution for the two conservation laws then gives the temperature and electric field; part of the energy is consequently emitted. To understand the distribution of the temperature in SPE container during the extrusion process, several assumptions were taken into account upon the numerical model

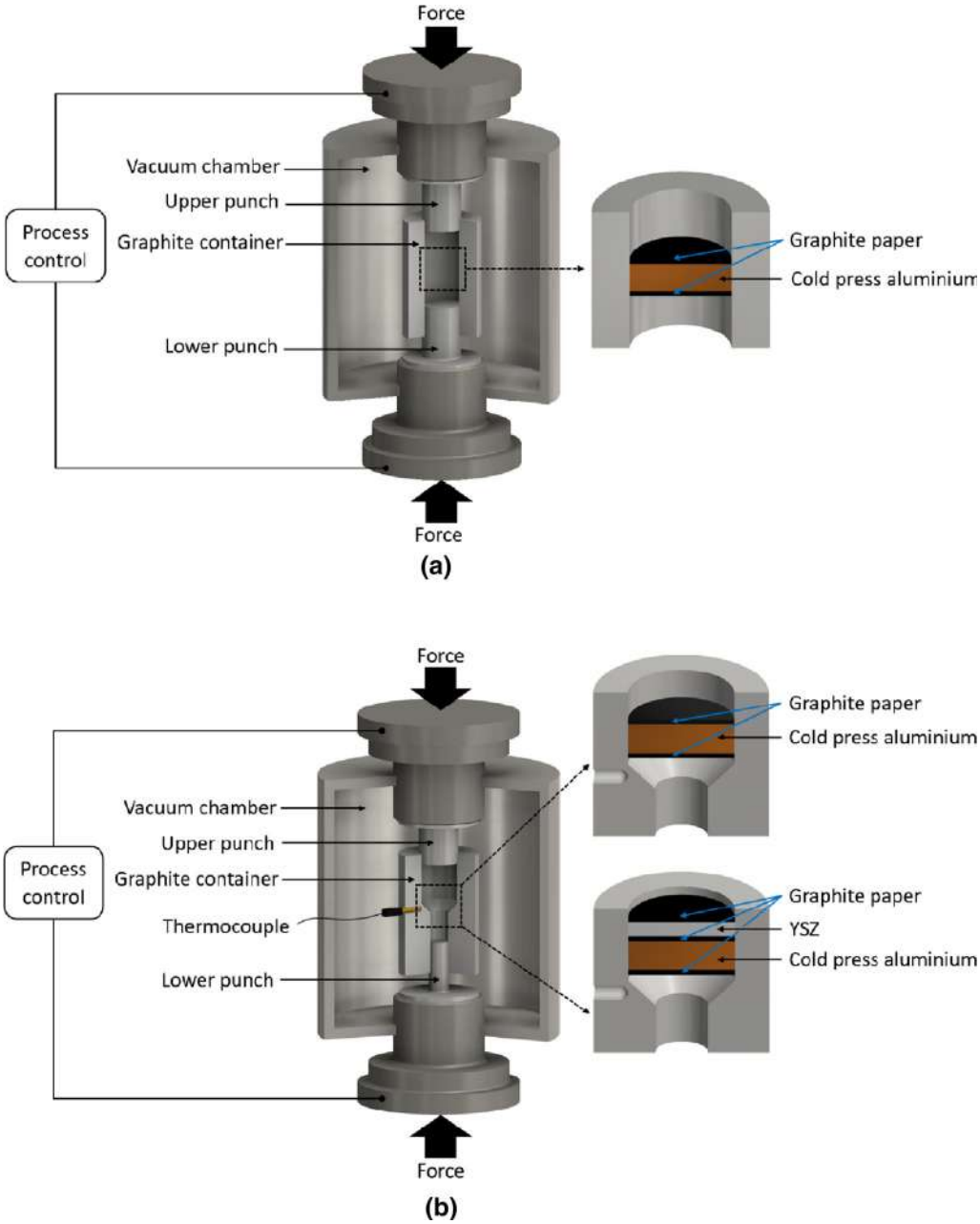

Fig. 1—Scheme of the container used for (*a*) cold press aluminum green-body manufacturing—position of the sample prior to the process, (*b*) spark plasma extrusion—position of the sample prior to the process.

calculation, *i.e.,* upper punch and graphite container are in thermal contact defined by its surface properties, no pre-compacted material was inserted into the SPE container, and the electric current was considered constant and direct. Other input conditions to the model, like electrical conductivity of graphite $\sigma c = 3000$ S/m, thermal conductivity kc = 150 W/mK, and emissivity of surface $\varepsilon c = 1$, were taken from COMSOL Multiphysics material library.

Extruded Al-CNTs samples for microstructural characterization were sectioned longitudinally, along the central axis in extrusion direction, using the deformation-free cutting apparatus Secotom 50 (STRUERS, Germany). Conventional procedure for the preparation of metallographic samples was applied, namely, grinding with water cooling, polishing with diamond pastes and Fuss's etchant (composition: 0.7 pct HF, 0.8 pct HNO_3, 2.4 pct HCl and 96.1 pct H_2O), were used to reveal the aluminum matrix composite grain boundary microstructure. Microstructural observation and acquisition of the images were performed by using a high-resolution 3D opto-digital light microscope DX510 (OLYMPUS, Japan). Detailed microstructures were recorded using scanning electron microscope Lyra3 (TESCAN, Czech Republic), and the chemical composition of selected areas in the metallographic samples was studied using Energy Dispersive X-ray (EDX) detector (Bruker XFlash 5010). The hardness HV 0.1

was measured along two lines, *i.e.,* in the vicinity of the edge and in the center of the extruded samples utilizing DuraScan 70 (STRUERS, Germany).

III. RESULTS AND DISCUSSION

A. *Description of Spark Plasma Extrusion (SPE) Process in an SPS Setup*

As mentioned earlier, one of the major advantages of our new setup is that extrusion can take place isothermally, since the graphite container remains heated during extrusion. Thus, the material inside the container does not experience temperature loss during extrusion, which has positive implications for the uniformity of the extruded material. As depicted in Figure 2(a), during the heating stage, which takes place prior the isothermal extrusion, the upper punch reaches a much higher temperature when compared with the graphite container; in fact, this temperature has been found to be almost three times higher than the melting point of pure aluminum (660.5 °C) reported by Massalski *et al.* in aluminum-based binary alloy phase diagrams.[16]

This overheating extreme is believed to be the result of poor contact between the upper punch and the SPE container, where the current density is localized in a small contact area (detailed explanation is provided in Section III–B). Nevertheless, the dwell at a temperature higher than the melting point of aluminum is present only during the first phase of the SPE process, and it promotes the formation of molten phase within the Al-CNTs green compact (containing micro-scale aluminum particles). Sun and Simon examined the melting behavior of aluminum particles and reported that by decreasing the particle size, the melting response moves towards lower temperatures.[17] Similarly, Čelko *et al.* have reported that thin aluminum sheets melted immediately when the temperature was within the range of 660 °C to 665 °C.[18] Since aluminum molten phase was formed locally (contact area between the graphite punch/container and aluminum), the extrusion of the samples was provided at considerably low extrusion pressure, and was ensured mostly by gravitation force transfer of the liquid phase; namely, from the top to the bottom part of the graphite container (see Figure 2(b)). This process as described herein is roughly related to vacuum-assisted low-pressure process used by Jiang *et al.*[19] or to high-pressure container casting process used by Niu *et al.*,[20] respectively, for the casting of aluminum alloys.

To enable the process of the solid-state spark plasma extrusion, a more uniform temperature distribution needs to be maintained. This can be achieved through our thermal barrier concept presented herein where an yttria partially stabilized zirconia (YSZ) powder layer, often used as a thermal barrier coatings (TBC), is applied between the top surface of the aluminum-CNT compact and the graphite punch. Darolia in a comprehensive review of thermal barrier coatings (TBCs) provided information on the layers of the TBC and explained the role of YSZ in TBC systems.[21] The thermal conductivity of aluminum is relatively high

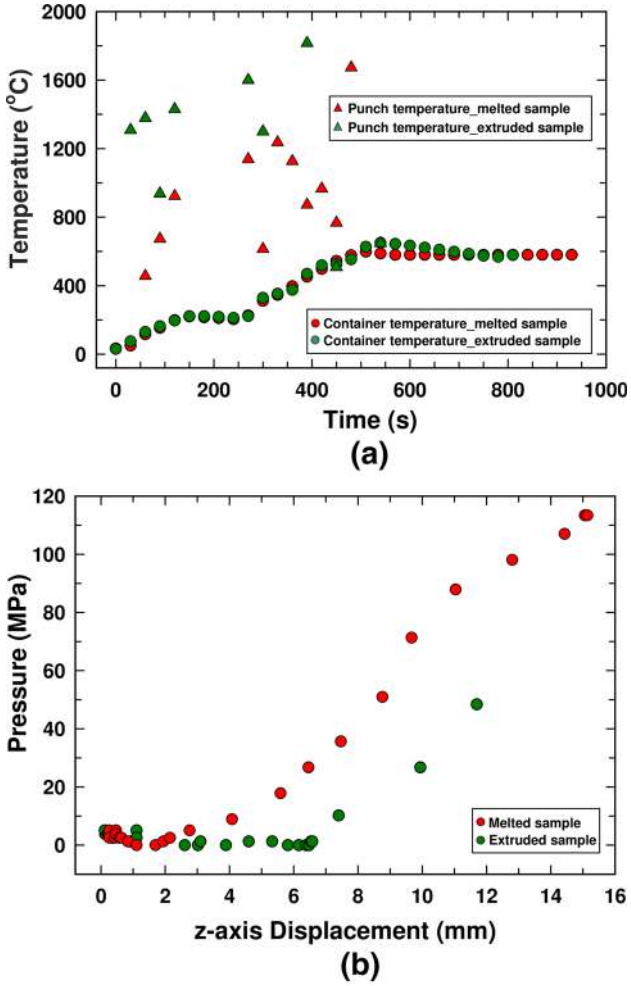

Fig. 2—Experimental data measured within the spark plasma extrusion process (*a*) plot of temperature *vs* time, (*b*) plot of extrusion pressure *vs* z-axis displacement.

(237 W/mK) as Molina *et al.* reported, *i.e.,* higher than that of YSZ.[22] The thermal conductivity of initial YSZ powder is not reported in the literature. However, Kyong studied the values of thermal conductivity of YSZ under different techniques including atmospheric plasma sprayed (APS).[23] For YSZ, the thermal conductivities lie within the range of 0.1 to 0.6 W/mK. As a result, the overheating extreme can be in general negated because of the relatively thin ceramic powder layer (0.2 to 1 mm), which is surrounded by graphite papers and is able to absorb the heat, to sinter as well as to promote the required drop in temperature.

After the desired extrusion temperature is reached, the compact is extruded by manually increasing the extrusion pressure. Note that the commercially available devices are designed only for the SPS process, and the force is set up at a constant value from the beginning of the process, and only rarely changes during the sintering. Conventional extrusion and SPE are strain controlled, and the force is applied during the process to maintain a constant ram extrusion speed. On the contrary as depicted in Figure 2(b), only a small increase in the extrusion pressure is required at the beginning of the SPE process,

which is followed by further and almost a constantly gradual increase in the extrusion pressure which is required until the expected length of the extruded material has been obtained. Previous work on SPE was conducted while initially maintaining extrusion container at room temperature. In these studies, the current was allowed to only pass through the powder compact by using an insulating mica sheet between the compact and the inner surface of the container. Such a setup results only in an increase in the temperature of the compact, through Joule heating. During extrusion, the main contributor to Joule heating which is the compact electrical resistance is reduced as the powder compact is densified and upset inside the extrusion chamber. Moreover, the contact between the extruding compact and the container (originally maintained at a much lower temperature) results in significant heat losses and a significant increase in extrusion pressure requirements. In our present work, having a container maintained at a high temperature results in low extrusion pressures compared with previous SPE work. If the process of extrusion stops, which can happen mostly due to discontinuity in the pressure increase, *i.e.,* the extruded material stays without the movement in extrusion direction inside the graphite container, it is almost impossible to continue the extrusion process without any damage to the container. The continuity of gradual increase in extrusion pressure is crucial especially in the case where some chemical interaction(s) of the surface can occur (*i.e.,* between the extruding material and graphite). Mackie *et al.* observed and reported this problematic behavior in the case of conventional SPS process for SmCo based magnets[24] and similarly Dudina *et al.* for the diffusion of carbon in Ni-W alloyed powders.[25]

B. *Model of Temperature Distribution in the SPE Container*

So far, Tiwari *et al.*[26] worked on the modeling of the conventional SPS process considered evolution of surface temperature, temperature distribution inside the sample and container, the electric field and heat flux. Voisin *et al.*[27] studied experimentally and theoretically the process to up-scaling in order to produce complex shapes of TiAl alloys. Also, Manière *et al.*[28] implemented the proportional integral derivative (PID) modeling to control the temperature in SPS process. Although such approaches have provided insights for SPS, a different approach is needed for SPE mainly due to the larger contact area of the punches and the container and geometric evolution of the extruding material. In this paper, we introduce a preliminary model to provide an insight into the temperature distributions within SPE and shed light on the observed extreme overheating of the punch within the heating stage of the SPE process. The initial small contact area of the punch with the rest of the container (the punch in 1 mm depth within the container) promotes a sharp local increase in the local current density and a corresponding rise in temperature due to Joule heating, as depicted in Figure 3.

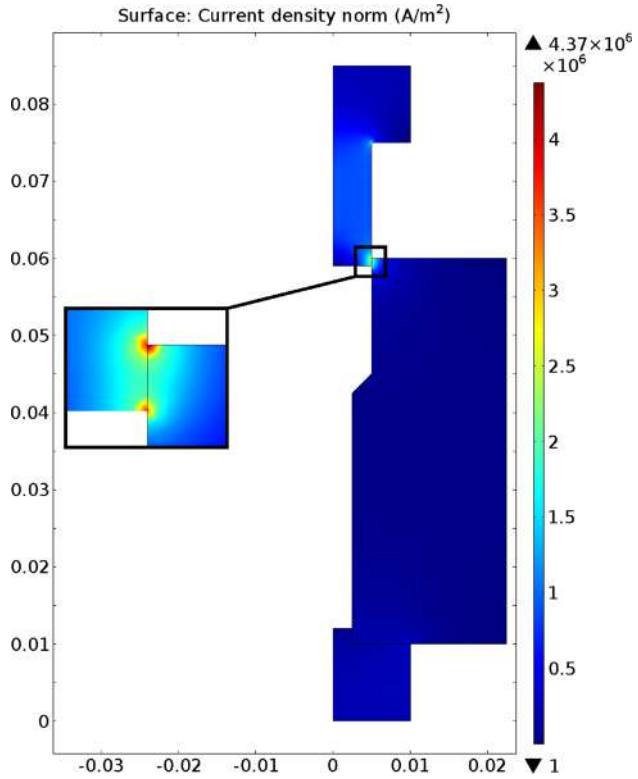

Fig. 3—Distribution of the current density during heating stage of the SPE process.

Song *et al.*[29] reported similar increases in current densities during neck formation of conducting powders during the early stages of the SPS process. As shown in Figure 4(a), the local increase in the current density results in the extreme overheating of the punch. The movement of the punch down the container during extrusion (*i.e.,* in the extrusion stage of SPE) promotes an increase in the contact area between the punch and container as it is shown in Figures 4(b) through (d), and better distribution in the current density and a decline in the temperature of the punch. At the same time, the graphite container transfers heat *via* radiation and conduction, and helps to provide a more homogenous temperature distribution between the punch and the container. In general, the simulation qualitatively confirms the punch overheating behavior which has been observed during this experiment.

C. *Spark Plasma Extrusion Without Thermal Barrier Concept*

As mentioned previously, the problem with the overheating of the upper punch in the designed graphite container for the SPE process leads to the melting of the Al-CNTs green compacts. Figure 5 shows a longitudinal cross-sectional image of the extruded material, including detailed micrographs of designated areas and hardness measured along the sample.

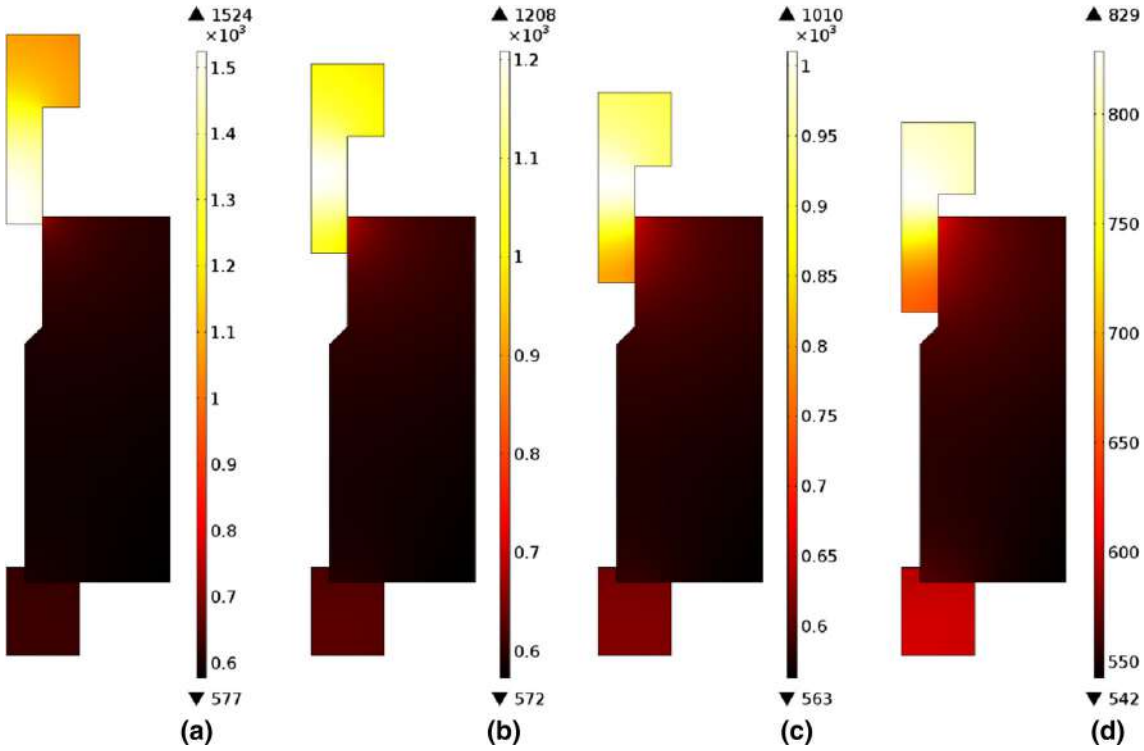

Fig. 4—Distribution of the temperature during extrusion stage of the SPE process; depth of the punch inside the container (*a*) 1 mm, (*b*) 6 mm, (*c*) 10 mm, (*d*) 14 mm.

From the overall image, the upper punch overheating and subsequent formation of molten aluminum during the SPE process which can be observed promotes the formation of two well-defined areas: (i) aluminum low in CNTs content (bright zone) and (ii) CNTs-rich area (dark zone). The shape and position of CNTs-rich area with respect to the extrusion direction and material flow marks suggest that separation of the carbon nanotubes is attributed to the melting of the aluminum during extrusion process. Also, the size of the main part of the CNTs-rich area approximately matches the displacement of the upper punch with minimal pressure increment at the beginning of the SPE process (see Figure 2b) when the liquid phase is transferred by gravitation from the top to the bottom part of the container.

Detailed images in Figure 5 were obtained using the differential interference contrast (DIC) method in order to enhance material flow and grain boundaries. As the CNTs distribution evidence was suppressed in these images, micrographs showing the CNTs distribution in Figure 5—areas 1, 3, 4, and 6, are also included. For the microstructural analysis, the sample can be divided into four different characteristic zones based on the microstructure and the physical process: (i) the sintered area, termed as SPS zone, located at the upper part of the container with a 10 mm diameter size. The material that stays in this area is sintered as in conventional SPS process and does not go through the deformation zone (*i.e.,* where the area is reduced by shearing); (ii) the deformation zone, which is located close to the central part of the container; (iii) the extrusion zone, which is located after the deformation zone and it is the part with the reduced diameter of 5 mm; (iv) the tip, which is located at the far end of the extruded material (*i.e.,* the first part to come out of the container exit).

Relatively coarse aluminum grains were observed in all zones of the melted material suggesting the absence of complete solid-state extrusion during the SPE process. In the extrusion zone, also very distinctive flow lines were observed as a result of the extrusion process. The central part of SPS zone (Figure 5—area 1) of the melted material demonstrated a larger polyhedral grains typical for characteristic SPS grain growth due to the higher temperature and pressure present in the area during the SPE process. The presence of such a microstructure in Figure 5—area 1 and not in the edge of SPS zone (Figure 5—area 2), suggests that the central part might not have melted during the extrusion process, unlike the edge of the SPS zone. As more factors are influencing the final microstructure (*e.g.,* temperature, applied pressure, compaction of powder, contact with the container), further experiments are necessary to prove this assumption.

The distribution of CNTs in Figure 5—areas 1, 3, 4, and 6 can be clearly seen from the comparison of both micrographs on the given areas. In SPS and tip zones of the material, CNTs are distributed along the grain boundaries while in the reduction and extrusion zones, the CNTs are distributed along the flow marks in the extrusion direction, regardless of the grain boundaries.

Figure 6(a) shows a representative scanning electron micrograph (SEM) of the interface between the CNTs-rich area and the Al matrix. Figure 6(b) displays the aluminum matrix area next to the interface. Darker dots are observed in the area and can be assigned to the

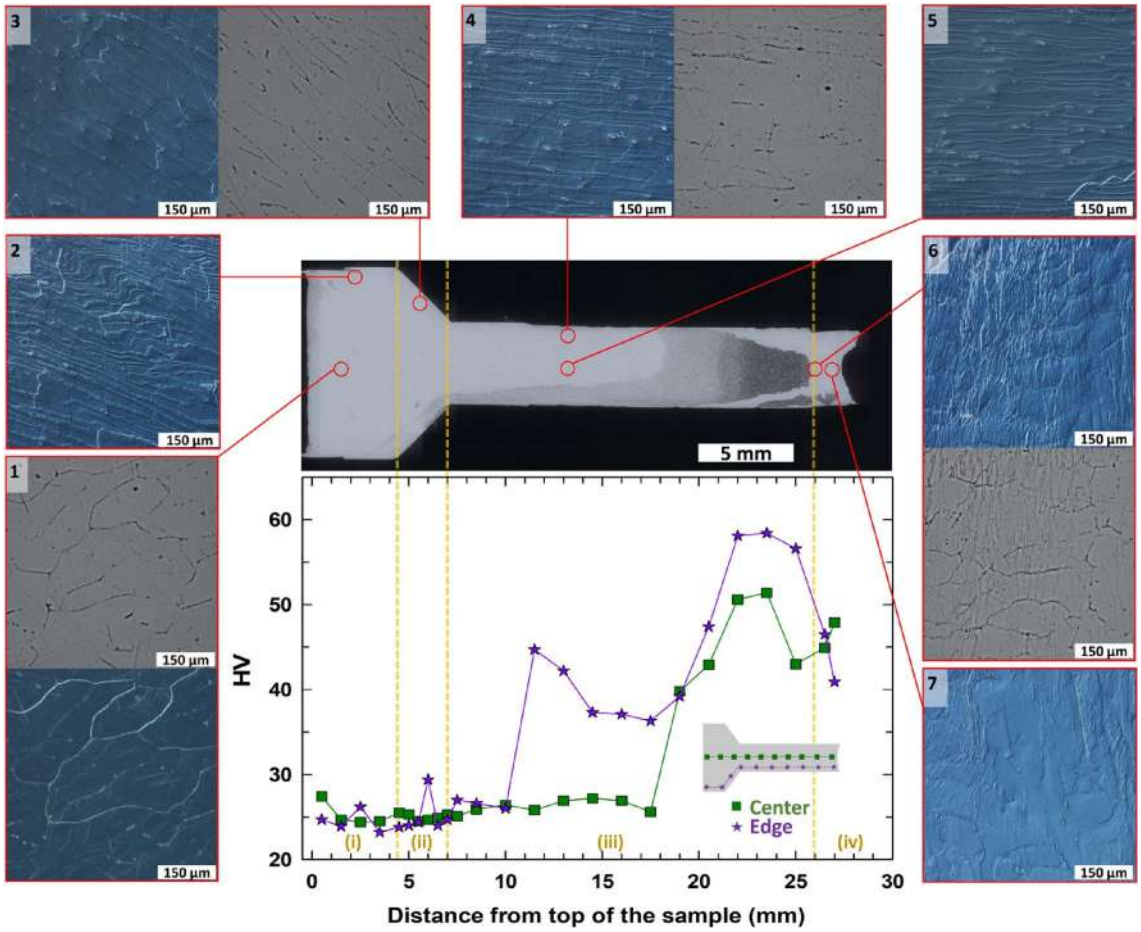

Fig. 5—Overall appearance and hardness measured along the Al-CNTs sample produced by SPE without implementation of thermal barrier concept; microstructures of (i) SPS zone, (ii) reduction zone, (iii) extrusion zone, and (iv) tip zone.

remaining CNT agglomerates. Agglomeration of CNTs in the CNTs-rich area in the metal phase melted during extrusion can be better observed from the more detailed micrograph in Figure 6(c). Local analysis of the chemical composition by EDX was performed. The area rich in CNTs presented a composition in atomic percentage of 90.4 pct of carbon and 5.6 pct of aluminum, compared to 7.4 pct of carbon and 92.2 pct of aluminum in the Al-CNTs area. For both areas, oxygen was also detected. This is expected due to the formation of a naturally protective layer, after the polishing of the sample surface.

The Vickers hardness data, shown in Figure 5, confirm the heterogeneity in composition and microstructure along the melted sample. The SPS zone of the sample, characterized by a conventional SPS process, shows an average value of 27.4 HV in the central part and a slightly lower average value of 24.3 HV is shown in the edge. Similar values were obtained in the reduction zone, namely 24.9 and 25.3 HV in the center and edge. Local increase of hardness up to nearly 30 HV was caused by the presence of CNTs-rich area along the edge of the melted sample. Hardness values in the edge and central part of the extruded zone remained similar to SPS zone and reduction zone, until a noticeable increase after approximately 4.5 and 11.0 mm, respectively. Both changes in hardness correspond to the transition from Al-CNTs area to CNTs-rich area. Further increase was observed in the darker part of the CNTs-rich area, probably due to the increase in CNT content. The highest hardness value obtained in CNTs-rich area was 58.4 HV. This value is comparable with Singla *et al.* reported hardness values for mechanical milling aluminum-CNT composites.[30] Therefore, the local CNTs volume fraction increased and contributed to the hardness observed. As it can be seen from the hardness evolution graph, the values at the central and edge area of the melted samples differ along the sample. This can be attributed to the many variables of the uncontrolled process due to the overheating of the upper punch which leads to partially melting of the material, *i.e.,* phase transformation, grain size and shape, recrystallization, and the pressure distribution in the material inside the graphite container.

D. *Spark Plasma Extrusion With Thermal Barrier Concept*

Once the YSZ layer is used to avoid the direct contact of the high temperature from the upper punch on the Al-CNTs green compacts, SPE was conducted without any significant complications. The use of the thermal

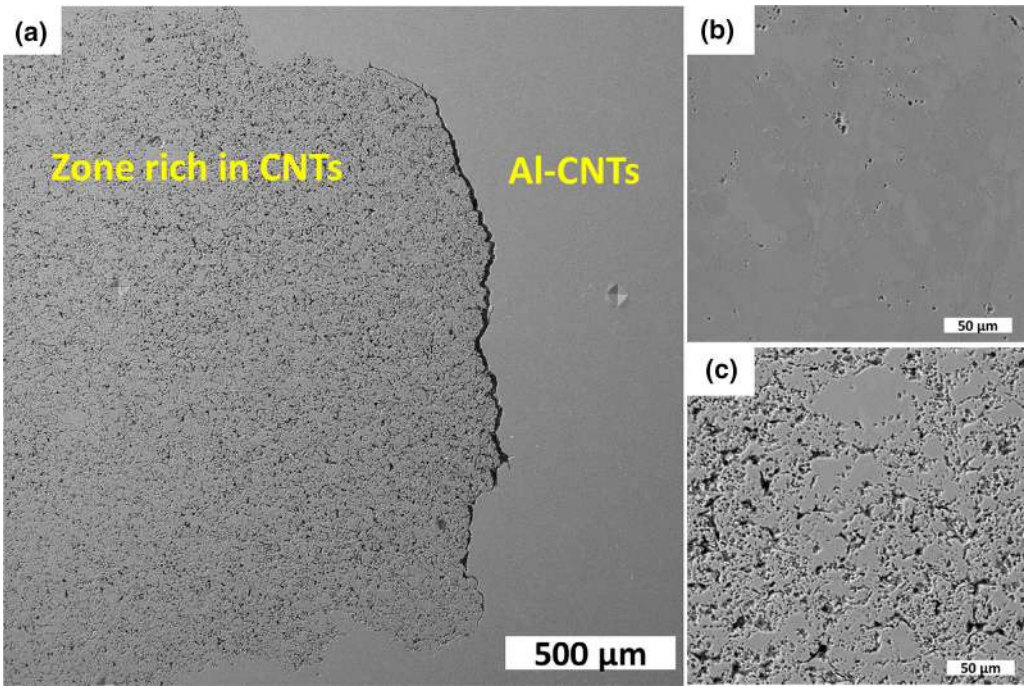

Fig. 6—Microstructure of Al-CNTs sample produced by SPE without implementation of thermal barrier concept: (*a*) the interface between the CNTs-rich area and the Al matrix, (*b*) Al matrix area next to the interface, (*c*) CNTs-rich area.

barrier concept results in a non-melted sample and the extrusion is achieved below the ceramic layer, as is depicted in Figure 7.

The homogeneity in the phase composition and the difference in shape of the grains along the extruded material are clearly observed. The non-extruded region (Figure 7—area 1) reveals a polyhedral grain structure. Kwon *et al*. observed similar microstructure of aluminum-CNT composite processed by SPS.[31] Similar microstructure can also be found in the tip of the extruded material. In this zone, the contacting pressure of the material against the bottom punch together with the temperature of the SPE process lead to a grain growth (Figure 7—area 6). An even higher pressure present during the process at the very end of the tip zone (Figure 7—area 7) results in flattening of the grains.

In the reduction and extrusion zones, the presence of crystallized aluminum from molten state was not observed. Moreover, the microstructure consists of grains elongated in the direction of extrusion and differs from finer to coarse from the surface (Figure 7—areas 3 and 4) to the center of the extruded sample (Figure 7—area 5). Also the flow marks are more distinctive in the subsurface area.

The distribution of CNTs in Figure 7—areas 1, 4, 6, and 7 can be clearly seen from the comparison of both the given micrographs of the areas. In all cases, the CNTs are distributed along the grain boundaries and no CNTs-rich area was observed along the sample. Also the hardness of the sample, presented in Figure 7, does not exhibit significant scatter of the data. Only marked increase was observed in the central area at the very end of the tip due to the high compaction in that area. Unlike the melted sample, the extruded material with the implemented thermal barrier concept, exhibited hardness values very close to each other, showing only a slight increment along the sample. For the SPS area, an average value of 34 HV was obtained for both the center and the edge areas, respectively. The reduction area is characterized by a small increment due to the plastic deformation of the material, and shows an average value of 35 and 36 HV in the center and the edge. Values obtained in SPS and reduction area were about 10 HV higher than those measured for the melted sample. This can be attributed to the proper extrusion process without complications (such as melting) which resulted in finer grains and a homogeneous microstructure. In the extruded area, the hardness further increased due to greater plastic deformation of the material and grain refinement. Lewandowska *et al*.[32] observed such behavior for solid-state extrusion of pure aluminum alloys and Kwon *et al*.[31] observed it as well for aluminum-CNT composites. Values were oscillating around 40 HV regardless of the indentation point distance from the top of the sample. The highest value is reported at the end of the tip zone (55.3 HV). Besides the higher compaction mentioned above, the inter-particle spacing between CNTs contributed to the observed hardness values. These values reported herein are comparable to those Morsi *et al*. reported earlier, for SPE-extruded Al-2.5 pct CNTs samples.[15] Such reduction in hardness can be attributed to the higher onset

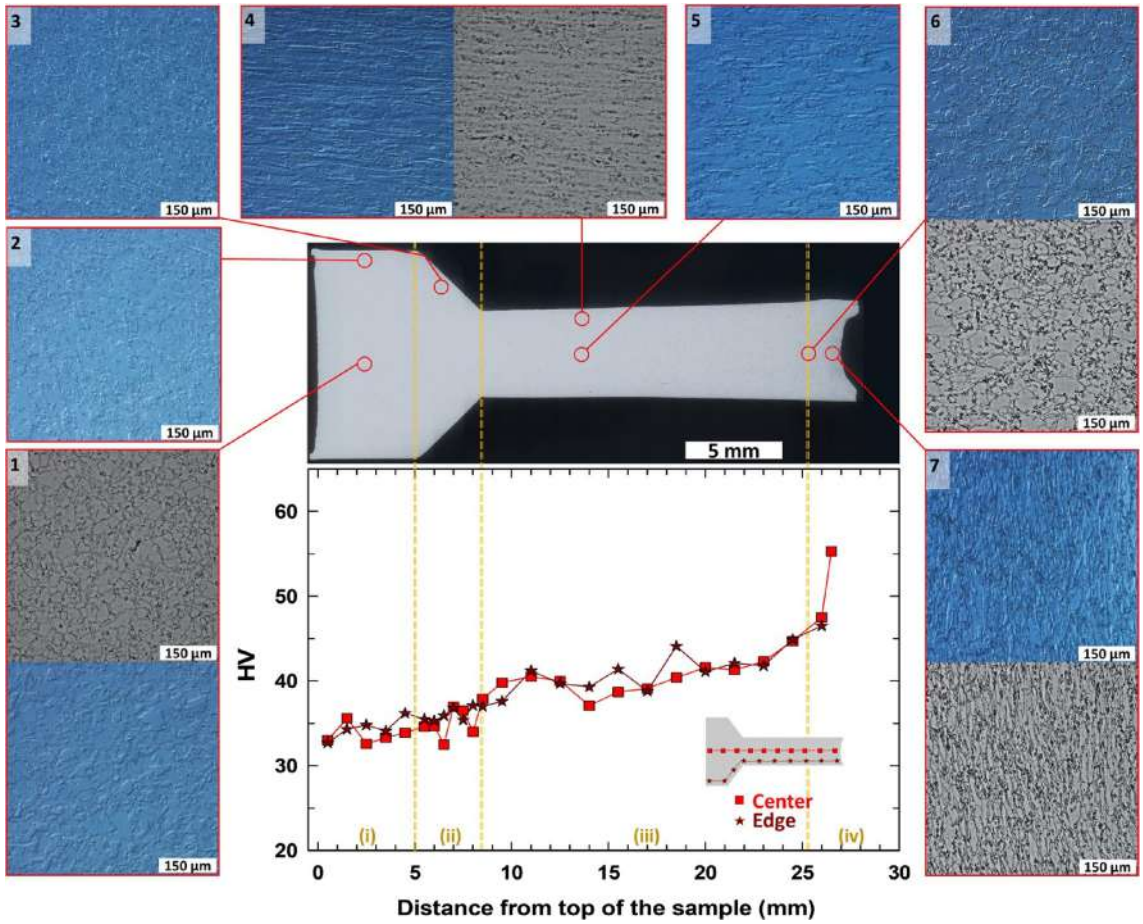

Fig. 7—Overall appearance and hardness measured along the Al-CNTs sample produced by SPE with implementation of thermal barrier concept; microstructures of (i) SPS zone, (ii) reduction zone, (iii) extrusion zone, and (iv) tip zone.

temperatures that were used in this study and therefore as Morsi *et al.* described due to possible dynamic recovery in the SPE process.[13]

IV. SUMMARY

In the present work, the thermal barrier concept for enabling a reproducible single-step spark plasma extrusion (SPE) manufacturing process within the commercially available SPS devices was introduced. SPE consists of the two continuous stages: (i) the heating stage and (ii) the extrusion stage, and a few differences in the process can be highlighted. Within the heating stage, the upper (extrusion) punch can reach temperatures almost three times higher than the melting point of pure aluminum. This extreme overheating is due to the very high current density localized at the upper punch and the graphite container interface. During the subsequent extrusion stage, the required pressure to continue the process of extrusion increases until the end of the SPE process.

Without utilizing the thermal barrier concept for processing of Al-CNTs composites, aluminum melts and results in a reverse dispersion of CNTs, into regions with high concentrations of CNTs and others of low concentrations. Materials spark-plasma-extruded without a thermal barrier possessed a heterogeneous microstructure and therefore, variations in hardness over the whole material.

By using the thermal barrier concept, the extreme overheating of the Al-CNTs green compact during the heating stage of SPE process was prevented and only solid-state extrusion takes place. In this case, the extruded material exhibited a homogeneous distribution of the CNTs within the aluminum matrix with grain refinement and hardness increase being observed. The results prove the feasibility of the thermal barrier concept in the SPE process which enables the single-step SPE processing of numerous powder-based material systems. Utilization of the SPE process for other metallic materials as well as metal matrix composites is currently under investigation.

ACKNOWLEDGMENTS

This work was financially supported by the Czech Science Foundation under the project GA 15-20991S. We also want to acknowledge access to the scanning electron microscopes provided within the frame of the

projects CEITEC 2020 (LQ1601) and CEITEC Nano RI, MEYES CR, 2016-2019.

REFERENCES

1. R. Orrú, R. Licheri, A.M. Locci, A. Cincotti, and G. Cao: *Mater. Sci. Eng. R*, 2009, vol. 63, pp. 127–287.
2. T. Grosdidier, G. Ji, and S. Launois: *Scripta Mater.*, 2007, vol. 57, pp. 525–28.
3. Z.A. Munir, U. Anselmi-Tamburini, and M. Ohyanagi: *J. Mater. Sci.*, 2006, vol. 41, pp. 763–77.
4. M. Tokita: *Pulse Electric Current Synthesis and Processing of Materials*, Wiley, New Jersey, NY, 2006, pp. 50–59.
5. M.A. Hussein, C. Suryanarayana, and N. Al-Aqeeli: *Mater. Des.*, 2015, vol. 87, pp. 693–700.
6. K.J. Kim, S.H. Jang, Y.W. Kim, B.K. Jang, and T. Nishimura: *Ceram. Int.*, 2016, vol. 42, pp. 17892–96.
7. V.R. Mudinepalli, S.H. Song, and B.S. Murty: *Scripta Mater.*, 2014, vol. 82, pp. 9–12.
8. M. Tokita: *Mater. Sci. Forum*, 1999, vols. 308–311, pp. 83–88.
9. X. Wang, S.R. Casolco, G. Xu, and J.E. Garay: *Acta Mater.*, 2007, vol. 55, pp. 3611–22.
10. S. Grasso, Y. Sakka, and G. Maizza: *Sci. Technol. Adv. Mater.*, 2009, vol. 10, p. 053001.
11. M. Tokita: US Patent No. 6383446, 2002.
12. K. Lichtinghagen: US Patent No. 4420294, 1983.
13. K. Morsi, A. El-Desouky, B. Johnson, A. Mar, and S. Lanka: *Scripta Mater.*, 2009, vol. 61, pp. 395–98.
14. E. Novitskaya, T.A. Esquivel-Castro, G.R. Dieguez-Trejo, A. Kritsuk, J.T. Cahill, S. Díaz-de-la-Torre, and O.A. Graeve: *Mater. Sci. Eng. A*, 2018, vol. 717, pp. 62–67.
15. K. Morsi, A.M.K. Esawi, P. Borah, S. Lanka, A. Sayed, and M. Taher: *Mater. Sci. Eng. A*, 2010, vol. 527, pp. 5686–90.
16. T.B. Massalski, H. Okamoto, P.R. Subramanian, and L. Kacprzak: *Binary Alloy Phase Diagrams*, 2nd ed., ASM International, Geauga County, OH, 1990.
17. J. Sun and S.L. Simon: *Thermochim. Acta*, 2007, vol. 463, pp. 32–40.
18. L. Čelko, S. Díaz-de-laTorre, L. Klakurková, J. Kaiser, B. Smetana, K. Slámečka, M. Žaludová, and J. Švejcarab: *Surf. Coat. Technol.*, 2014, vol. 258, pp. 95–101.
19. W. Jiang, Z. Fan, D. Liu, D. Liao, X. Dong, and X. Zong: *Mater. Sci. Eng. A*, 2013, vol. 560, pp. 396–403.
20. X.P. Niu, B.H. Hu, I. Pinwill, and H. Li: *J. Mater. Process. Technol.*, 2000, vol. 105, pp. 119–27.
21. R. Darolia: *Int. Mater. Rev.*, 2013, vol. 58, pp. 315–48.
22. J.-M. Molina, M. Rheme, J. Carron, and L. Weber: *Scripta Mater.*, 2008, vol. 58, pp. 393–96.
23. J.A. Kyong: *Mater. Trans.*, 2014, vol. 55, pp. 188–93.
24. A.J. Mackie, G.D. Hatton, H.G.C. Hamilton, J.S. Dean, and R. Goodall: *Mater. Lett.*, 2016, vol. 171, pp. 14–17.
25. D.V. Dudina, B.B. Bokhonov, A.V. Ukhina, A.G. Anisimov, V.I. Mali, M.A. Esikov, I.S. Batraev, O.O. Kuznechik, and L.P. Pilinevich: *Mater. Lett.*, 2016, vol. 168, pp. 62–67.
26. D. Tiwari, B. Basu, and K. Biswas: *Ceram. Int.*, 2009, vol. 35, pp. 699–708.
27. T. Voisin, L. Durand, N. Karnatak, S. Le Gallet, M. Thomas, Y. Le Berree, J.F. Castagné, and A. Couret: *J. Mater. Process. Technol.*, 2013, vol. 213, pp. 269–78.
28. C. Manière, G. Lee, and E.A. Olevsky: *Results Phys.*, 2017, vol. 7, pp. 1494–97.
29. X. Song, X. Liu, and J. Zhang: *J. Am. Ceram. Soc.*, 2006, vol. 89, pp. 494–500.
30. D. Singla, K. Amulya, and Q. Murtaza: *Mater. Today Proc.*, 2015, vol. 2, pp. 2886–95.
31. H. Kwon, M. Estili, K. Takagi, T. Miyazaki, and A. Kawasaki: *Carbon*, 2009, vol. 47, pp. 570–77.
32. M. Lewandowska and K. Kurzydlowski: *J. Mater. Sci.*, 2008, vol. 43, pp. 7299–7306.